

A LEVEL-SET METHOD FOR THE EVOLUTION OF FACETED CRYSTALS*

GIOVANNI RUSSO[†] AND PETER SMEREKA[‡]

Abstract. A level-set formulation for the motion of faceted interfaces is presented. The evolving surface of a crystal is represented as the zero-level of a phase function. The crystal is identified by its orientation and facet speeds. Accuracy is tested on a single crystal by comparison with the exact evolution. The method is extended to study the evolution of a polycrystal. Numerical examples in two and three dimensions are presented.

Key words. level-set methods, crystals

AMS subject classifications. 65C20, 82D25

PII. S1064827599351921

1. Introduction. It is well established that under certain conditions gases and liquids solidify into faceted crystals. By faceted we mean that the surface is piecewise flat. The evolution of the crystal is often described by the motion of its surface, which is uniquely determined once its normal velocity, v_n , is known. In general v_n may depend on a wide variety of parameters such as orientation, curvature, adatom concentration, and temperature. In some situations the growth depends only on the orientation of the facets. This is called the van der Drift model [1, 2, 3]. In other situations the growth is controlled by curvature. For faceted crystals the curvature effects can be modeled by using crystalline curvature; for more details see Taylor [4, 5].

An example where the speed of the surface depends only on the orientation of the facets is given to a good approximation by diamonds grown by chemical vapor deposition. The (111) and (100) planes can grow at different speeds. The speed ratio determines the characteristics of the surface of the final crystal.

In this work we shall consider the situation where v_n depends only on orientation and the evolution of the interface is determined from

$$(1.1) \quad \dot{\mathbf{x}} = \gamma(\mathbf{n})\mathbf{n}.$$

If the function $\gamma(\mathbf{n})$ is smooth and convex, then an initially smooth curve remains smooth. If $\gamma(\mathbf{n})$ is not convex, then singularities will develop on the surface. For detailed explanations of these phenomena, see [6, 7]. In physical situations the formation of facets is observed. In particular, Wulff and Frank studied the asymptotic shape of a crystal, subject to a given $\gamma(\mathbf{n})$ law of motion [26]. Wulff proposed a method to predict the shape. This method amounts to using the inner convex hull of $\gamma(\mathbf{n})$ or, equivalently, the Legendre transformation of $\gamma(\mathbf{n})$. This shape is called the Wulff shape. Frank [10] proposed a different construction which gives the same answer. These constructions are well explained in [6, 7, 14].

*Received by the editors February 10, 1999; accepted for publication (in revised form) September 16, 1999; published electronically May 17, 2000. This work was supported in part by the National Science Foundation through Mathematical Sciences Career grant DMS-9625190, by DARPA and ONR through the Virtual Integrated Prototyping (VIP III) initiative, and by CNR-NSF joint grant N.97.00181.CT01.

<http://www.siam.org/journals/sisc/21-6/35192.html>

[†]Department of Mathematics, University of L'Aquila, L'Aquila, Italy (russo@univaq.it).

[‡]Department of Mathematics, University of Michigan, Ann Arbor, MI 48109 (psmerek@umich.edu).

Wettlaufer, Jackson, and Elbaum devised a Lagrangian numerical method to evolve a faceted seed which gives the correct Wulff shape [25]. A level-set method based on (1.1) has been proposed by Osher and Merriman; see [13]. In their formulation the interface is taken to be the zero-level set of a continuous function. Then they solved the following PDE:

$$(1.2) \quad \frac{\partial \phi}{\partial t} + \gamma \left(\frac{\nabla \phi}{|\nabla \phi|} \right) |\nabla \phi| = 0.$$

A similar formulation has been used by Taylor, Cahn, and Handwerker (consult [6, 7]).

Existence and uniqueness of such an equation are obtained in the framework of viscosity solutions for Hamilton–Jacobi equations. Using this formulation, under general assumptions, Osher and Merriman were able to prove that an initial interface asymptotically approaches the Wulff shape associated to the $\gamma(\mathbf{n})$ law [13]. Earlier, Soravia [21] proved this result by a different approach. More recently Peng et al. [14] used a numerical scheme based on this formulation to evolve an interface toward the Wulff shape. They also explored the connection between motion of faceted interfaces and motion of shocks for conservation laws. Another approach similar in spirit to the level-set approach is based on phase field methods. There have been a number of interesting papers on the evolution of faceted interfaces in this context (see, for example, [22, 23, 11, 9]).

To use the formulation given by (1.2) for interface evolution, one needs to provide an initial shape and a $\gamma(\mathbf{n})$ law for all directions \mathbf{n} . On the other hand, in many practical cases, the Wulff shape is a fully faceted surface. In this case the Wulff shape is determined by the speeds of the facets, and the speeds in other directions are irrelevant to the dynamics once the crystal is completely faceted. Thus, in the case of fully faceted crystal having a speed law for all directions is something of a mathematical convenience. In experimental situations only the speed of each facet can be measured, therefore to use the framework given by (1.2) one must find a $\gamma(\mathbf{n})$ (which is not unique) for all angles such that its Wulff shape agrees with experimental measurements. This is a relatively simple task for regular polyhedra in two dimensions but it does not seem so simple in three dimensions.

In this paper we propose an alternate level-set approach for the numerical computation of completely faceted crystals. This method only requires the velocity of each facet. In some sense the method automatically finds a $\gamma(\mathbf{n})$ which has the correct Wulff shape. As we shall see our approach is very closely connected with the work found in [13] and [14], and in fact it should be viewed as an extension of that work. In addition we also explore the evolution of polycrystals; each seed has its own level-set function corresponding to the crystal orientation. When the crystals touch they do not merge, but instead a grain boundary is formed.

2. Facet evolution. Each facet has a plane associated with it. The plane moves with a given normal speed, which may be different for different facets. The boundaries of the facets are determined by the intersection of the planes. The two-dimensional (2D) evolution near a corner is shown in Figure 1. If we use a level-set method where the normal speed is a simple interpolation between the two normal speeds, then the corners would be rounded, as is shown in Figure 2. (In particular, they would be arc of a circle if the two speeds are the same.) In order to keep flat facets and sharp corners, we make the following observation. The evolution of a smooth curve depends only on the normal speed, and the addition of a tangential component has the effect of just changing the parameterization of the curve. We evolve the front with a velocity that

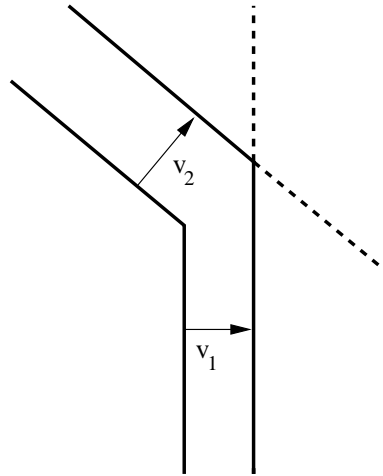


FIG. 1. Facet evolution near a corner in two dimensions.

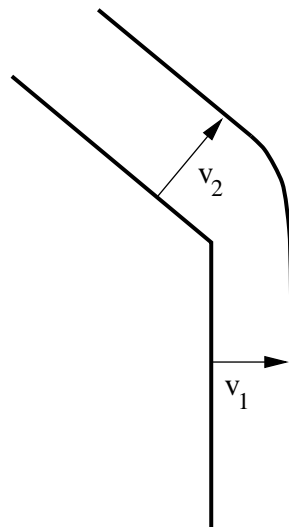


FIG. 2. Evolution near a corner when the normal speed at the corner is a linear interpolation of the normal speeds of the two facets.

has a component tangential to the facet and is directed toward the corner. With a proper tangential velocity (which can be determined by the construction in Figure 1) the facets will evolve, maintaining sharp corners. For example, for $v_1 = v_2$ and a square corner, the necessary tangential velocity which has to be added on both sides of the corner is v_1 . Note that this is a lower bound for the tangential velocity. In fact, if we move the points with a tangential velocity which is greater than this value, then the evolution of the interface will be the same. The addition of the tangential velocity causes the characteristics to collide; the solution does not become multivalued because we will use standard techniques for viscosity solutions to the Hamilton–Jacobi equation. This causes a shock to form and the corner stays sharp (see Figure 3). Note

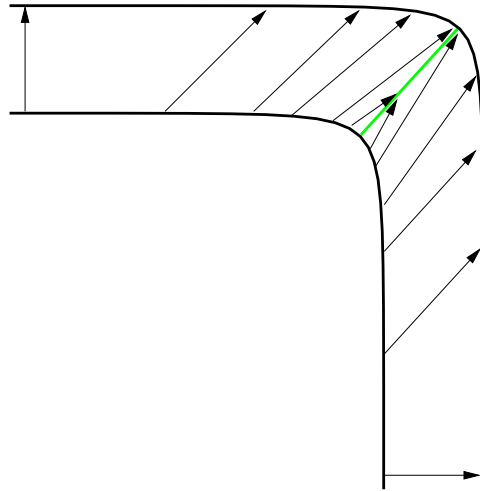


FIG. 3. Addition of a velocity component tangential to the facets maintains sharp corners.

that the velocity that we add is tangential to the facet, not to the interface. This has the effect of modifying the normal component of the interface if the latter is not aligned along a facet. In this respect the method can be viewed as a technique to construct a proper normal velocity law $\gamma(\mathbf{n})$, given the facet speeds.

2.1. Computation of the tangential velocity. In the approach that we use, the speed of each facet must be specified. The crystal will have M facets, with normals and normal speeds denoted by $\boldsymbol{\nu}_m$ and w_m with $m = 1, \dots, M$. Let \mathbf{n} be the normal at a given point to the interface, which will be denoted by Σ .

In order to compute the proper velocity of the surface at a given point, we first select the facet which is closest in direction to \mathbf{n} , i.e., for which $\mathbf{n} \cdot \boldsymbol{\nu}_m$ is maximum,

$$(2.1) \quad k = \arg \max_m \mathbf{n} \cdot \boldsymbol{\nu}_m.$$

Next we define the following velocity:

$$(2.2) \quad \mathbf{v} = w_k \mathbf{n} + u \boldsymbol{\tau},$$

where

$$(2.3) \quad \boldsymbol{\tau} = \frac{\mathbf{n} - (\mathbf{n} \cdot \boldsymbol{\nu}_k) \boldsymbol{\nu}_k}{[|\mathbf{n} - (\mathbf{n} \cdot \boldsymbol{\nu}_k) \boldsymbol{\nu}_k|^2 + \varepsilon^2]^{1/2}}$$

and u is the tangential speed, which will be specified below. The parameter ε in the denominator is a numerical parameter which ensures that $\boldsymbol{\tau}$ vanishes smoothly when the numerator vanishes.

Simple geometric considerations show that at a corner between two facets, the tangential speed that must be added to keep the corner sharp satisfies the following relation (see Figure 4):

$$u_{12}^\perp = \frac{w_2 - w_1 \cos \alpha}{\sin \alpha}.$$

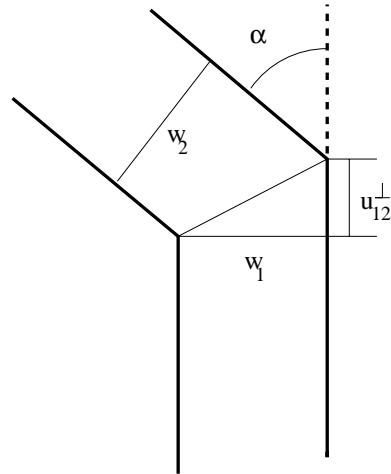


FIG. 4. Minimal transverse velocity necessary to keep corners sharp.

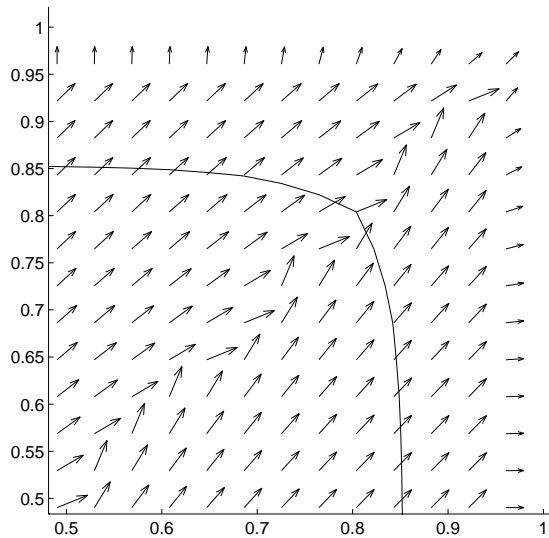


FIG. 5. Vector field \mathbf{v} associated to a given surface.

Then the quantity u can be chosen equal to u^* , where

$$(2.4) \quad u^* = \max_{i,j} u_{ij}^\perp, \quad \text{with side } i \text{ neighbor of side } j, \text{ and } w_j \geq w_i.$$

For a faceted interface, $\tau = 0$ because $\mathbf{n} = \nu_k$ and the face will evolve with the standard normal speed. On the other hand, if we evolve the whole interface with velocity $\mathbf{v} = w_k \mathbf{n}$, then the corners would get rounded and the evolution would be the one shown in Figure 2. When the corners become slightly rounded, then τ becomes directed toward the corner and the surface will move with a velocity that will try to keep the corners sharp. The effect of formula (2.2) is illustrated in Figure 5. By

choosing a small value for ε , the vector $\boldsymbol{\tau}$ is basically a unit vector whenever \mathbf{n} is not aligned with the facets. Neglecting ε , the normal velocity of our model is given by

$$(2.5) \quad \gamma(\mathbf{n}) = w_k + u\sqrt{1 - (\mathbf{n} \cdot \boldsymbol{\nu}_k)^2}.$$

It is essential that the γ law provides the correct Wulff shape. We conjecture that (2.5), with $u \geq u^*$, satisfies this condition. On the other hand, if $u < u^*$, then portions of the crystal interface will be curved.

As a 2D example, we consider a seed with four facets, with normals $(1, 0)$, $(0, 1)$, $(-1, 0)$, $(0, -1)$, and normal speeds all equal to 1. For this situation, $u^* = 1$. In Figure 6 we have plotted the Wulff shape corresponding to (2.5) for three values of u . It is clear that for $u = 0.55$ the Wulff shape is not a square, but for $u \geq 1$ it is.

Our next example consists of a seed with four facets with the same normals as in the previous example, but with speeds $w = 2, 1, 2, 1$. In Figure 7 we have shown the polar plot of $\gamma(\mathbf{n})$ (2.5), with $u = 2.2$ (in this case $u^* = 2$), together with its Wulff shape.

We remark that the transient evolution of a smooth initial surface rests on the detailed dependence of v_n on \mathbf{n} , but two $\gamma(\mathbf{n})$ which have the same Wulff shape will give identical evolution laws for fully faceted crystals. In this respect, no particular physical meaning is attached to expression (2.5): it is just a technique to compute the correct evolution law of faceted interfaces. Note that the function (2.5) is not necessarily continuous, as we have seen in the above example. However, this is not a problem for computation, as we shall see later in the paper.

2.2. Polycrystals. Typically, many crystals grow from individual seeds, each of them growing as a faceted crystal. Each individual crystal will grow until it hits another crystal, forming a grain boundary. Once formed, a grain boundary moves on a much longer time scale. In our model we shall assume that grain boundaries do not move.

3. Level-set framework. In the level-set approach for a single crystal we introduce a continuous function $\phi(\mathbf{x}, t)$, such that the crystal interface Σ is given by

$$(3.1) \quad \Sigma = \{\mathbf{x} | \phi(\mathbf{x}, t) = 0\}.$$

Thus we see that the zero-level set of ϕ is the interface; furthermore, we take $\phi < 0$ inside the crystal and $\phi > 0$ outside. The unit normal on the interface is given by

$$\mathbf{n} = \frac{\nabla\phi}{|\nabla\phi|}$$

evaluated at $\phi = 0$. The velocity of the interface is given by

$$(3.2) \quad \begin{aligned} \mathbf{v} &= w_k \mathbf{n} + u \boldsymbol{\tau} \\ &= w_k \frac{\nabla\phi}{|\nabla\phi|} + u \frac{\nabla\phi - (\boldsymbol{\nu}_k \cdot \nabla\phi) \boldsymbol{\nu}_k}{(|\nabla\phi - (\boldsymbol{\nu}_k \cdot \nabla\phi) \boldsymbol{\nu}_k|^2 + \tilde{\varepsilon}^2)^{1/2}}, \end{aligned}$$

where $\tilde{\varepsilon} = \varepsilon |\nabla\phi|$, and $k(\mathbf{x}, t) = \arg \max_m \boldsymbol{\nu}_m \cdot \nabla\phi$. This expression, when evaluated at $\phi = 0$, gives the same velocity defined in the previous section. We note that this velocity field is defined in the whole region Ω , and therefore it can be used to evolve the phase ϕ according to the equation

$$(3.3) \quad \frac{\partial\phi}{\partial t} + \mathbf{v} \cdot \nabla\phi = 0.$$

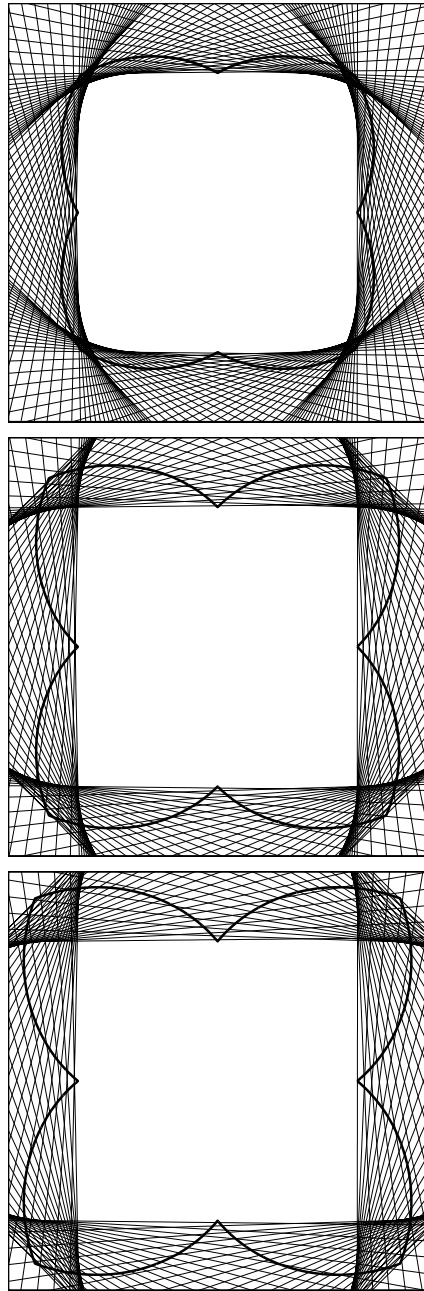


FIG. 6. Gamma law and corresponding Wulff shape. $\gamma(\mathbf{n})$ (thick line) is given by (2.5) and the Wulff shape is the envelope of the straight lines (see [6, 14]). The values of u are 0.55, 1.0, and 1.2 (from top to bottom).

With this evolution law, the zero-level set of $\phi(\mathbf{x}, t)$ will describe the evolution of the interface.

At time $t = 0$, the phase function is initialized so that $\phi(\mathbf{x}, 0)$ is continuous and

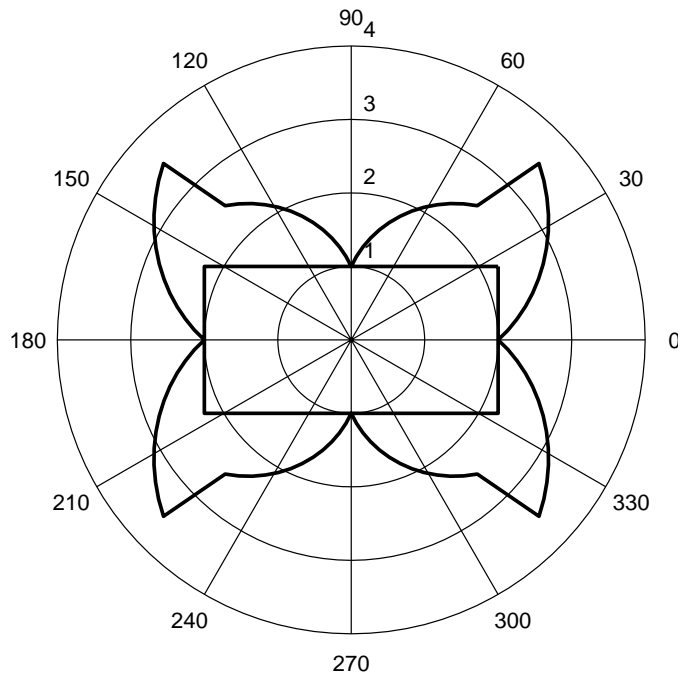


FIG. 7. Polar plot of the normal velocity and the corresponding Wulff shape.

$$\begin{aligned} \phi(\mathbf{x}, 0) &< 0 && \text{inside the crystal,} \\ \phi(\mathbf{x}, 0) &> 0 && \text{outside the crystal.} \end{aligned}$$

4. Polycrystal and grain boundaries. The previous method can be extended to describe the evolution of several crystals. Let us assume we have N_c crystal seeds. In this case we assign a different phase function $\phi_\ell, \ell = 1, \dots, N_c$ to each crystal. Each phase evolves with equation

$$(4.1) \quad \frac{\partial \phi_\ell}{\partial t} + \eta \mathbf{v}_\ell \cdot \nabla \phi_\ell = 0$$

and the velocity field \mathbf{v}_ℓ is computed as in the 1-crystal case. When two phase boundaries touch, then their evolution speed is set to zero, i.e., $\eta = 0$.

5. Numerical implementation. We use two different numerical methods to solve (3.2)–(3.3). They are both based on upwind methods on a fixed square grid. If all the initial seeds lie within the computational domain, then the velocity field on the boundary points outward, and therefore no boundary conditions have to be prescribed. Such approaches are typical for level-set methods (consult [16, 18]).

5.1. Single phase.

Method 1. In the first scheme we calculate the velocity \mathbf{v} by using center difference approximation for $\nabla \phi$, for example,

$$\frac{\partial \phi}{\partial x}(x_i, y_j, t_n) \approx \frac{\phi_{i+1,j}^n - \phi_{i-1,j}^n}{2\Delta x},$$

and then ϕ is updated by a first-order upwind method,

$$\phi_{i,j}^{n+1} = \phi_{i,j}^n - \Delta t(u_{i,j} D_x^{\text{upw}} \phi + v_{i,j} D_y^{\text{upw}} \phi).$$

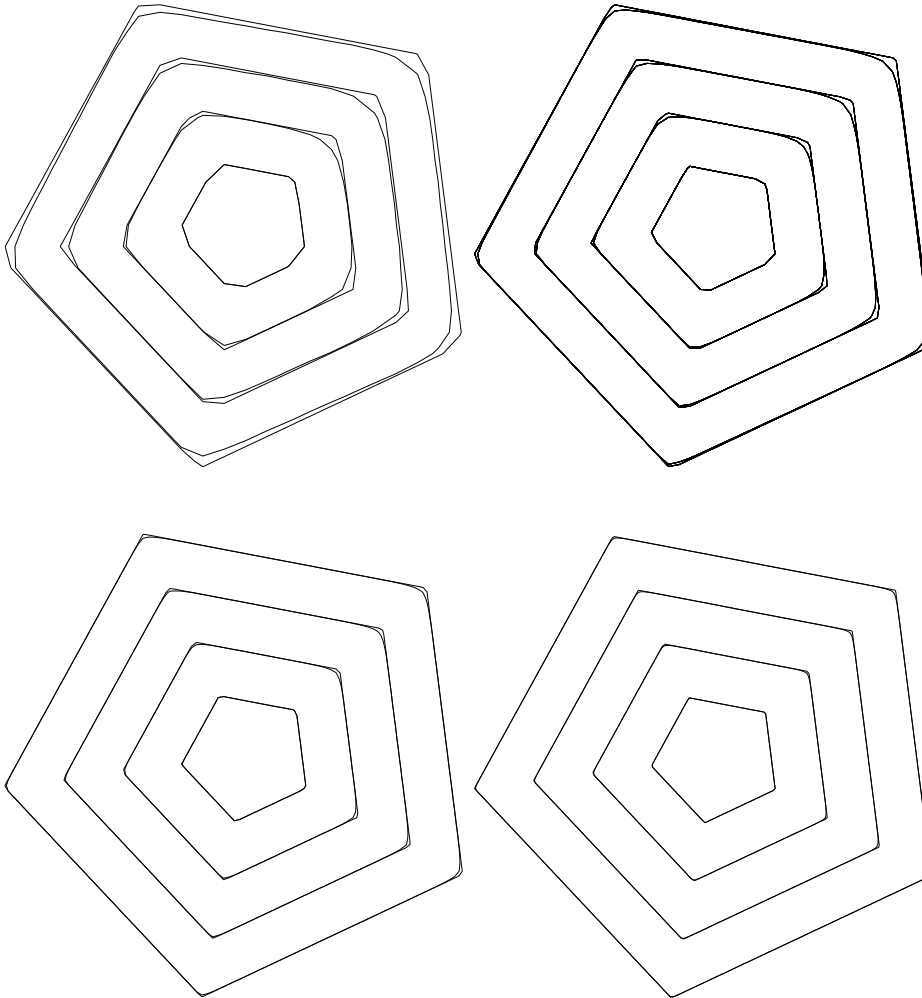


FIG. 8. Contour plots of the zero level-set at different times and comparison with exact solution. Grids: 25×25 , 50×50 , 100×100 , 200×200 .

In the above expression $u_{i,j}$ and $v_{i,j}$ are, respectively, the x and y components of \mathbf{v} given by (3.2), where derivatives of ϕ are computed with center differences; further we have

$$D_x^{\text{upw}} \phi_{i,j} = \begin{cases} D_x^b \phi_{i,j} & \text{if } u_{i,j} > 0, \\ D_x^f \phi_{i,j} & \text{if } u_{i,j} \leq 0, \end{cases}$$

with

$$D_x^b \phi_{i,j} = \frac{\phi_{i,j} - \phi_{i-1,j}}{\Delta x} \quad \text{and} \quad D_x^f \phi_{i,j} = \frac{\phi_{i+1,j} - \phi_{i,j}}{\Delta x},$$

and a similar formula holds for D_y^{upw} .

The method developed here presents some resemblance to the method of artificial compression of Harten [8]. In that case, the characteristic velocities across a discontinuity are artificially altered in order to make the discontinuities sharper.

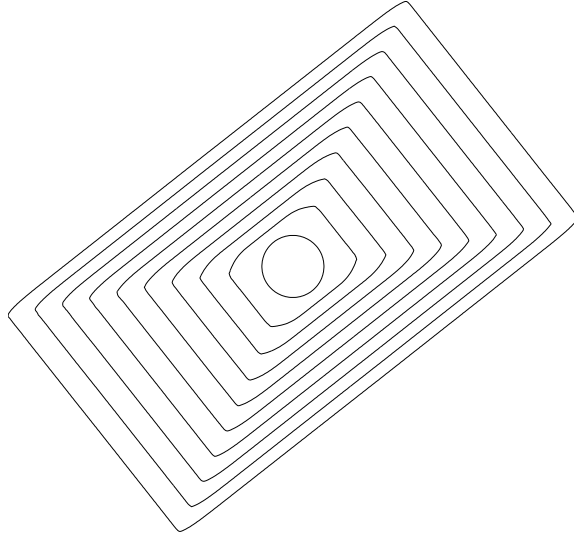


FIG. 9. The initial condition is a circle. The normal speeds of the faces are 1 and 2, and we have used $u = 2.2$.

Method 2. The second scheme is based on writing the equation in a Hamilton–Jacobi form, and using a modification of the scheme proposed by Rouy and Tourin [17]. First we rewrite the equation as

$$\frac{\partial \phi}{\partial t} + F(\nabla \phi) |\nabla \phi| = 0,$$

where the normal speed $F(\nabla \phi)$ is given by

$$(5.1) \quad F = \mathbf{v} \cdot \mathbf{n} = \mathbf{v} \cdot \frac{\nabla \phi}{|\nabla \phi|}$$

and the velocity \mathbf{v} is given by (3.2). Equation (5.1) is discretized as follows: We compute the velocity \mathbf{v} using centered differencing as before and the normal speed is then approximated as

$$F_{i,j} = \frac{u_{i,j} D_x^{\text{upw}} \phi + v_{i,j} D_y^{\text{upw}} \phi}{\sqrt{(D_x^{\text{upw}} \phi)^2 + (D_y^{\text{upw}} \phi)^2 + \varepsilon^2}}.$$

Next the phase function ϕ is updated according to

$$(5.2) \quad \phi_{i,j}^{n+1} = \phi_{i,j}^n - \Delta t g F_{i,j},$$

where

$$g = \begin{cases} \sqrt{\max(|(D_x^b \phi)_+|, |(D_x^f \phi)_-|)^2 + \max(|(D_y^b \phi)_+|, |(D_y^f \phi)_-|)^2} & \text{if } F_{i,j} > 0, \\ \sqrt{\max(|(D_x^b \phi)_-|, |(D_x^f \phi)_+|)^2 + \max(|(D_y^b \phi)_-|, |(D_y^f \phi)_+|)^2} & \text{if } F_{i,j} \leq 0, \end{cases}$$

and for any real number h , $(h)_+ \equiv \max(h, 0)$ denotes the positive part and $(h)_- \equiv \min(h, 0)$ denotes the negative part. We remark that this latter method is very similar in spirit to the method used by Peng et al. [14] and it may be viewed as an automatic way to compute $\gamma(\mathbf{n})$ (see [13, 14]).

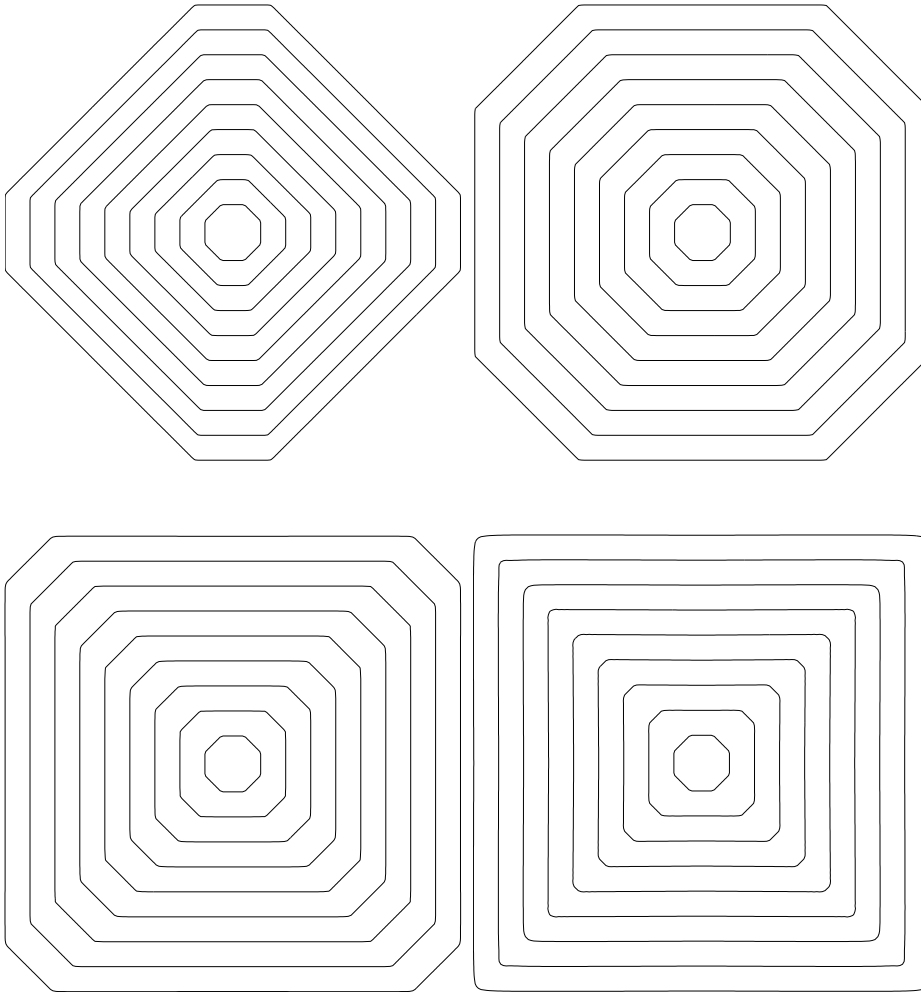


FIG. 10. Contour plots of the zero level-set at different times. Velocity ratio v_{11}/v_{10} : 0.8, 1.1, 1.3, 1.5. Grid size: 200×200 .

5.2. Multiple phases. Multiple phases are handled in much the same way as we handle a single seed except we must make a modification when two phases touch and a grain boundary forms. We discretize (4.1) as follows: First compute a candidate for the new phase, according to (5.2),

$$\phi_{i,j}^*(\ell) = \phi_{i,j}^n(\ell) - \eta_{i,j}^n \Delta t F_{i,j} g,$$

where $\phi_{i,j}^n(\ell) = \phi_\ell(x_i, y_j, t_n)$. $\phi_{i,j}^{n+1}(\ell)$ is computed from $\phi_{i,j}^*(\ell)$ once it has been determined whether or not grain boundary has formed. This is done in two steps explained below.

Step 1. Computation of η . When two phases meet, they stop moving. This is obtained computationally as follows:

$$\eta_{i,j}^{n+1} = \begin{cases} 0 & \text{if any of the phases } \phi_{i,j}^*(\ell) \text{ overlap,} \\ 1 & \text{otherwise.} \end{cases}$$

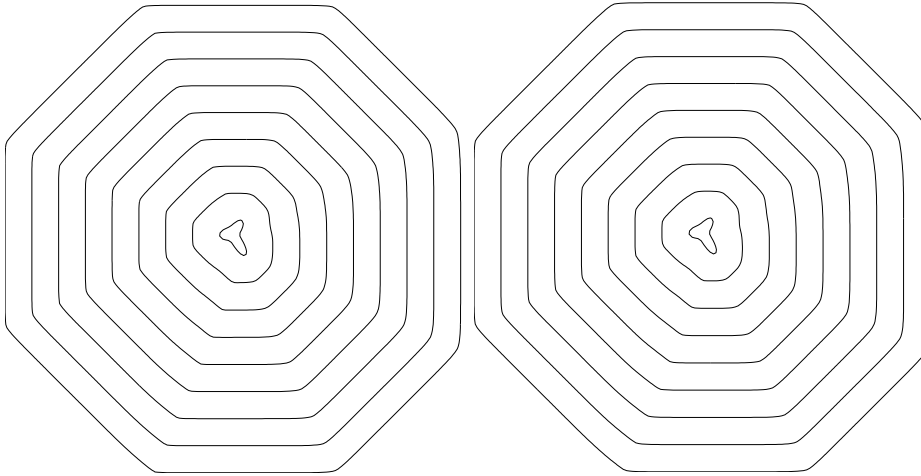


FIG. 11. Contour plots of the zero level-set at different times. The initial condition is a smooth nonconvex curve. The figure on the left is computed using Method 1 (with $u = .45$), whereas the one on the right is computed with Method 2. A 200×200 grid has been used.

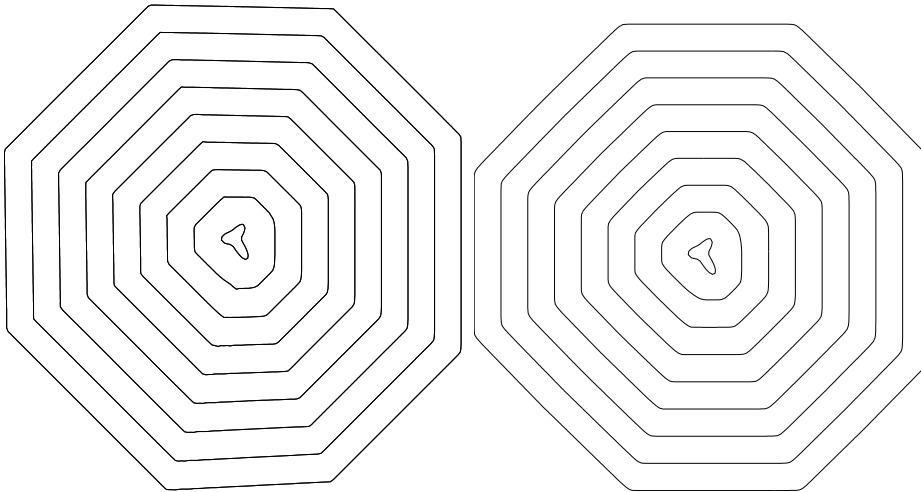


FIG. 12. Contour plots of the zero level-set at different times. The initial condition is a smooth nonconvex curve. The figure on the left is computed using Method 1 (with $u = 1.0$), whereas the one on the right is computed with Method 2. A 200×200 grid has been used.

Phases are said to overlap at grid point (i, j) if $\phi_{i,j}^*(\ell_1) \leq 0$ and $\phi_{i,j}^*(\ell_2) \leq 0$ for any pair (ℓ_1, ℓ_2) , $\ell_1 \neq \ell_2$.

Step 2. Computation of grain boundary. When two phases meet, to ensure that the phases do not pass through each other we compute the new phase as follows:

$$\phi_{i,j}^{n+1}(\ell) = \begin{cases} \tilde{\phi}_{i,j}(\ell) & \text{if phase } \ell \text{ overlaps with another phase,} \\ \phi_{i,j}^*(\ell) & \text{otherwise.} \end{cases}$$

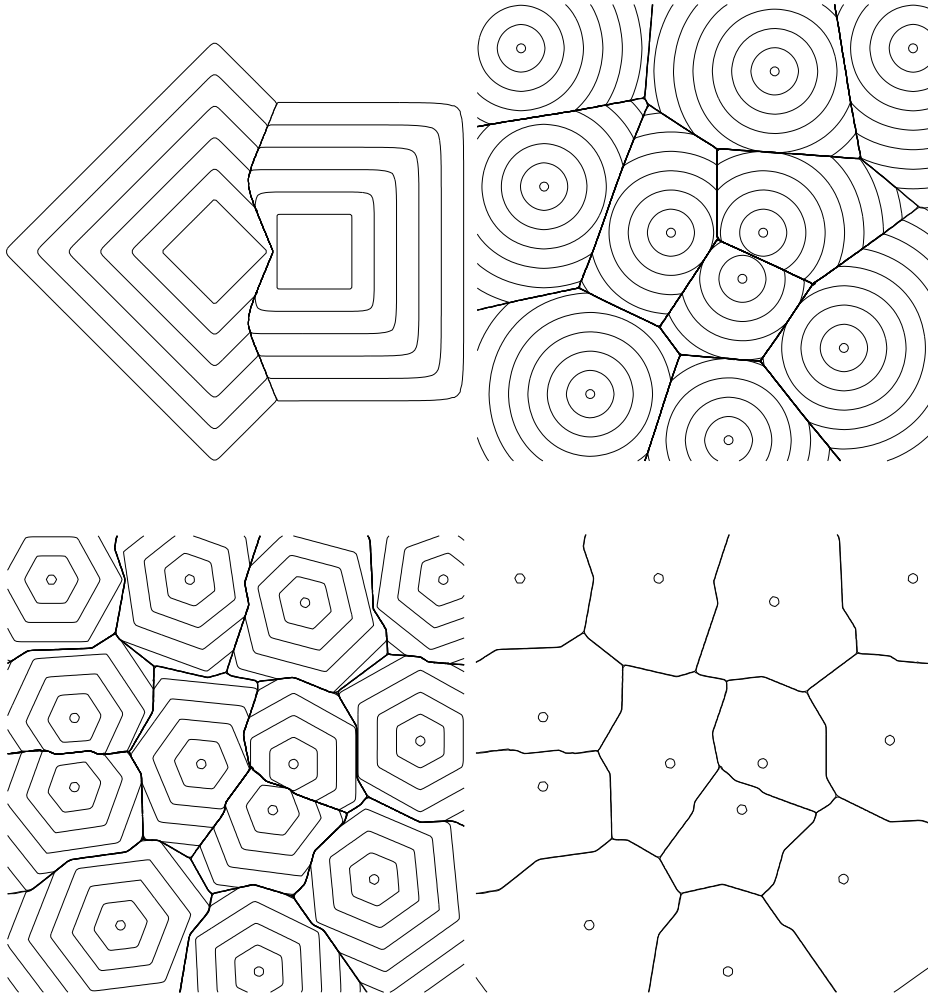


FIG. 13. *Formation of grain boundaries: (a) growth of two square seeds; (b) growth of isotropic seeds and formation of the Voronoi diagram at grain boundaries; (c) growth of hexagonal seeds and formation of polycrystal; (d) same as previous picture, but only seeds and grain boundaries are shown.*

$\tilde{\phi}_{i,j}$ is computed as follows: we consider two overlapping phases ℓ_1 and ℓ_2 with $\ell_1 < \ell_2$ and define

$$\begin{aligned} \tilde{\phi}_{i,j}(\ell_1) &= \frac{1}{2}(\phi_{i,j}^*(\ell_1) - \phi_{i,j}^*(\ell_2)), \\ \tilde{\phi}_{i,j}(\ell_2) &= \frac{1}{2}(\phi_{i,j}^*(\ell_2) - \phi_{i,j}^*(\ell_1)). \end{aligned}$$

This step ensures that there is a grain boundary between two phases ℓ_1 and ℓ_2 , that is to say ϕ_{ℓ_1} and ϕ_{ℓ_2} are both zero on the same set. Note that this procedure only compares pairs of phases. Triple points are automatically captured by the method, although there might be a slight dependence of the location of the triple point on the order in which the pairs of phases are swept. An alternate procedure has been

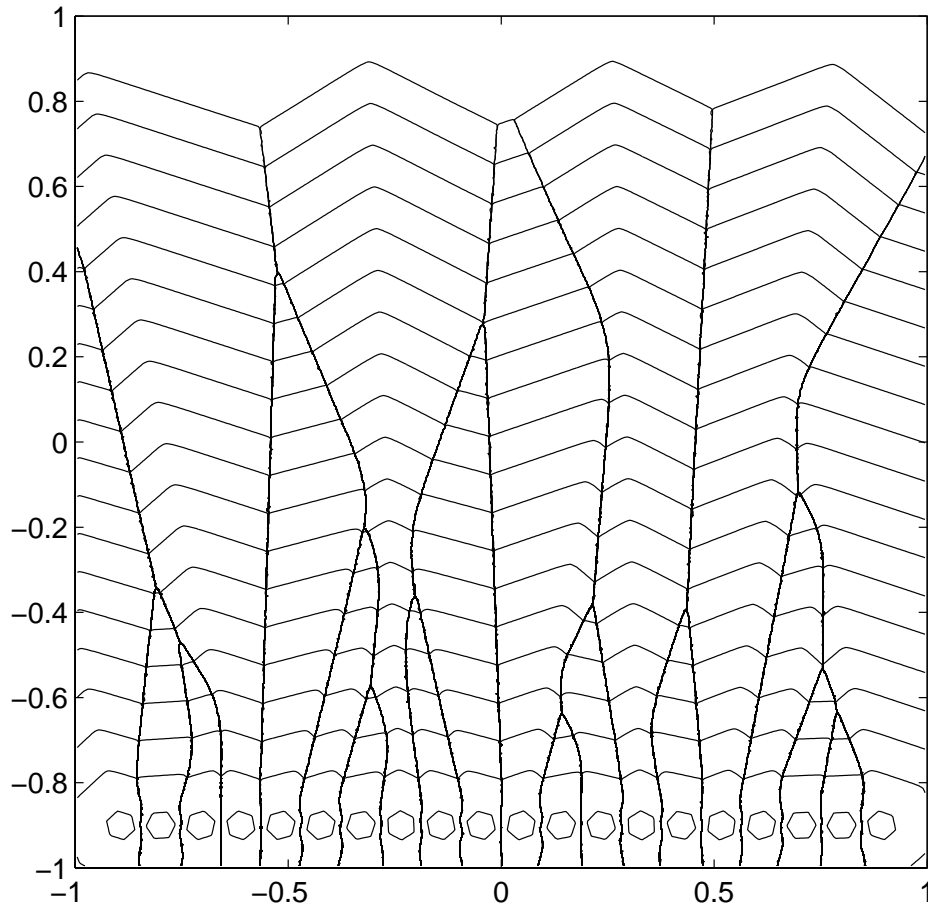


FIG. 14. *Natural selection. Growth of hexagonal seeds. The seeds with an orientation which gives the fastest speed of propagation in the y direction will survive.*

considered by Merriman, Bence, and Osher in their study of multiple junctions [15].

6. Numerical results. In this section we show the results of some tests in two and three dimensions.

2D tests. First we want to examine the resolution of the schemes. We consider the evolution of a pentagonal seed and compare the exact solution with the numerical solution obtained by Method 1. The result is shown in Figure 8. The exact solution is obtained by the contour plot of the exact phase function on the same grid used for the numerical calculation. On a 200×200 grid the numerical and exact contours practically overlap. Increasing the magnitude of the tangential component u does not affect the results other than sharpening the corners. Method 2 produces similar results with slightly more rounded corners.

In the second example we return to the situation described in section 3, where γ is plotted in Figure 7. In this case the Wulff shape is a rectangle and γ is a discontinuous function of \mathbf{n} . Nevertheless we see that our method provides the correct solution (see Figure 9). The computation is performed using Method 2.

As a third example we consider the growth of an octagonal seed, for various values

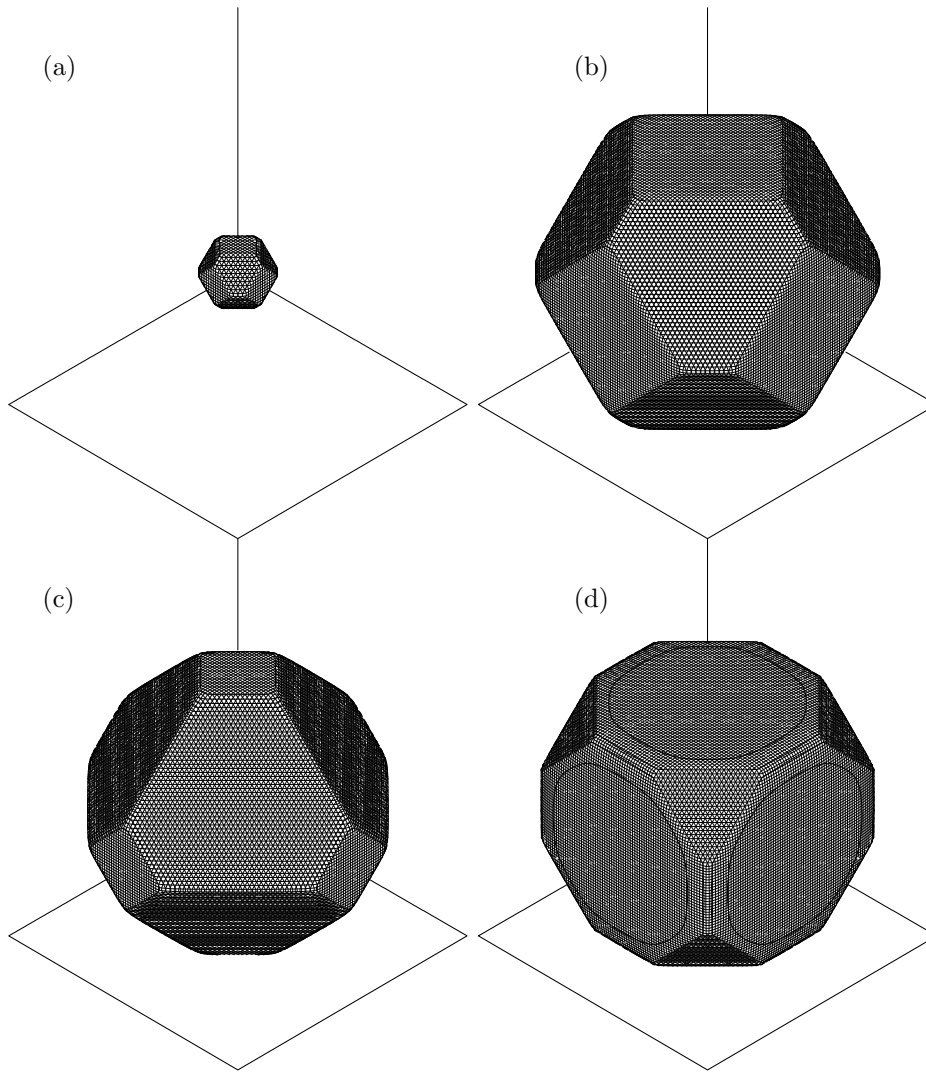


FIG. 15. Growth of a diamond crystal in three dimensions, for various values of v_{111}/v_{100} ratio at $t = .56$ (a) Initial seed; (b) $v_{111} = 1.2, v_{100} = 1.2$; (c) $v_{111} = 1.0, v_{100} = 1.4$; (d) $v_{111} = 1.4, v_{100} = 1.0$.

of the speed ratios v_{11}/v_{10} . For speed ratio between $1/\sqrt{2}$ and $\sqrt{2}$ the Wulff shape is an octagon (regular only if $v_{11}/v_{10} = 1$), while outside of this range it becomes a square. The results of the computation for Method 1 are shown in Figure 10.

In the next test we consider the evolution of different seeds corresponding to the same crystal. In this case the crystal has eight facets and the speeds are all the same. The Wulff shape is a regular octagon. According to theory, the shape of the crystal approaches the Wulff shape asymptotically in time (see, for example, [13]). In Figure 11 we show the evolution of a smooth nonconvex irregular seed obtained with the two methods. The speeds of the facets are all 1.0 and the tangential speed u is 0.45. The figure shows that the two methods give essentially the same result, which is in agreement with theory.

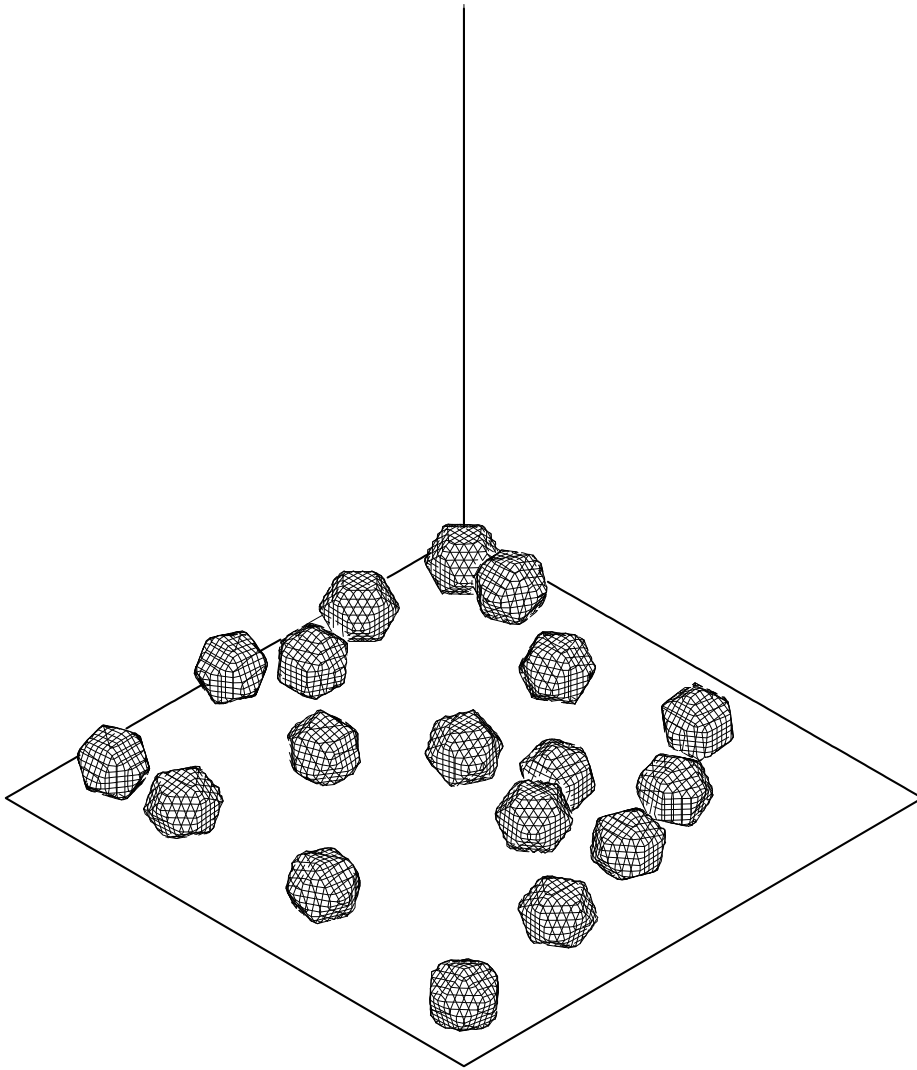


FIG. 16. *Growth of 18 seeds in three dimensions. Each seed is the same as that in Figure 15 except each seed has been rotated by a random amount. Here $v_{111} = 1.0$ and $v_{111}/v_{100} = 1.4$. This shows the initial condition.*

There is a small problem with Method 1, however. This occurs when the magnitude of the tangential velocity, u , is too large and the initial seed is not faceted and convex. This drawback is displayed in Figure 12, where we show results of both methods when the magnitude of the tangential velocity is $u = 1$. It is clear that with Method 1 the solution is not approaching the Wulff shape, whereas the solution computed with Method 2 is. We suspect the reason for this is that Method 1 is not a monotone scheme. For this reason we use Method 2 in all subsequent calculations. It is well known that the viscosity solutions to Hamilton–Jacobi equations are unique. Monotone schemes are known to produce numerical solutions that converge to the viscosity solutions. Lack of monotonicity may result in convergence to a solution that is not a viscosity solution.

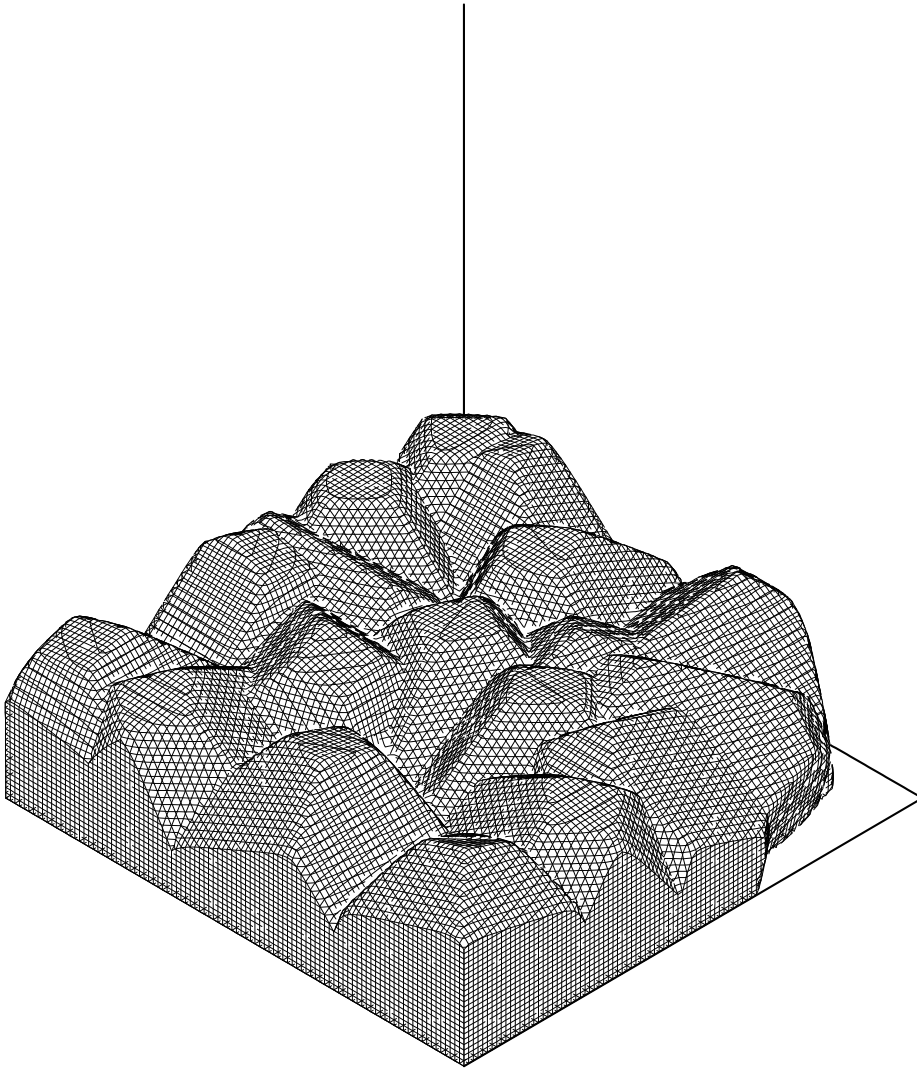


FIG. 17. Same as Figure 16, except $t = 0.28$.

The next tests are devoted to the evolution of several seeds and formation of grain boundaries. In Figure 13 we show several examples of grain boundary formation. The first picture shows the evolution of two square seeds, corresponding to a crystal with four facets, all with the same speed. The lines represent the crystal surface at different times. In the second picture, the evolution of the surface corresponding to isotropic growth is shown. The initial seeds are small circles with the same radius; they grow isotropically with the same speed. The grain boundaries in this case form the Voronoi diagram associated with the center of the seeds. In the third picture we show how the method can be used to study the formation of a polycrystal. In this case the Wulff shape of the crystal is a regular hexagon. All the crystals start with a small seed randomly placed in the plane and with random orientation. In the last picture only the seeds and the final grain boundaries are shown.

A similar situation was examined by Kobayashi, Warren, and Carter [19] using

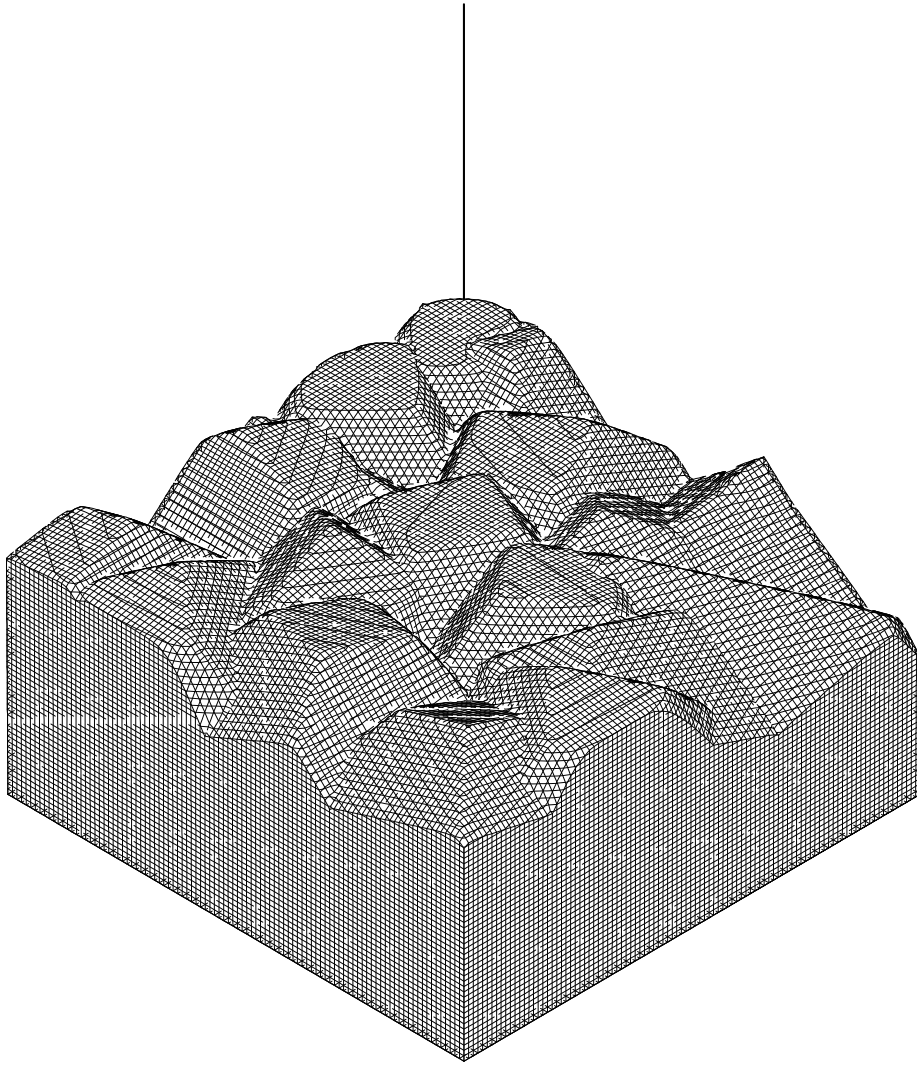


FIG. 18. Same as Figure 16, except $t = 0.56$.

a vector-valued phase field model. They studied the growth of a large number of seeds. Their model not only captured their dynamics of the growth of the seeds but also the resulting grain boundaries. In addition their model allows the inclusion of a large number of physical effects. In a related study Chen and Yang [20] use a set of Ginzburg–Landau equations to model the evolution of grain boundaries. They observe that the microstructure coarsens.

A more realistic model of crystal growth should specify the law according to which the initial seeds are created. When spontaneous nucleation is neglected and when the fraction of impurities of the material is low enough, a reasonable model consists of placing a certain number of initial seeds near one of the boundaries and then letting them grow. A 2D simulation of such a growth is shown in Figure 14. In this case a certain number of seeds corresponding to hexagonal crystals are initially placed near the bottom. When two phases meet, the grain boundary evolves at the intersection

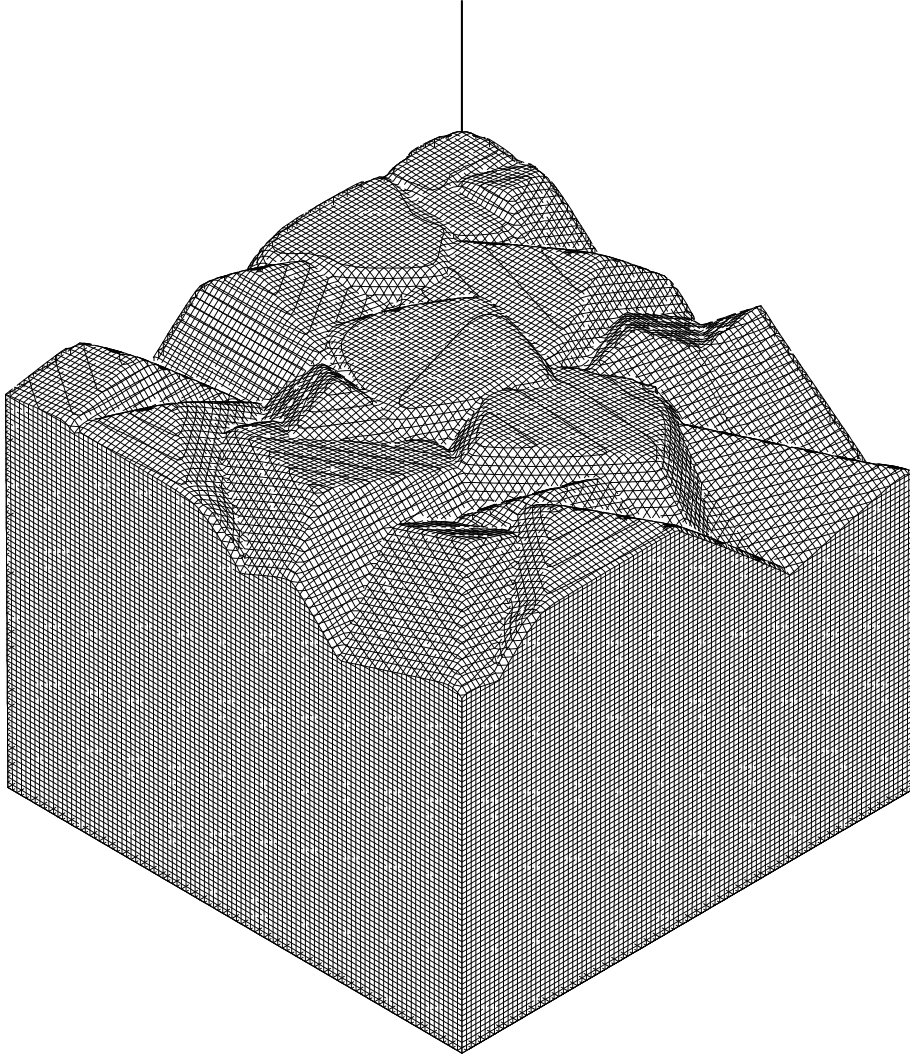


FIG. 19. Same as Figure 16, except $t = 0.98$.

of the two phases. There is an analogy between grain boundary and shocks. The evolution of the grain boundary is the same as the evolution of a shock formed by the intersection of two characteristics aligned along the normal to the surfaces Σ_ℓ . If all the propagation speeds are the same, then the direction of the growth is aligned along the bisector of the angle formed by the two phases. When two grain boundaries meet, they merge into one. Because of their merging and of their geometric property, a “natural selection” takes place as the crystal grows and only the seeds which allow grain boundaries aligned with the direction of growth will survive. This corresponds to seeds whose corners are oriented near the direction of growth (see Figure 14).

This problem has been studied using a vertex tracking approach by Paritosh et al. [2]. They study in detail the coarsening phenomena and compute various statistical properties of the evolving microstructure. In particular they show that the number of grains scale like $t^{-1/2}$. In addition, Thijssen, Knops, and Dammers [24] and

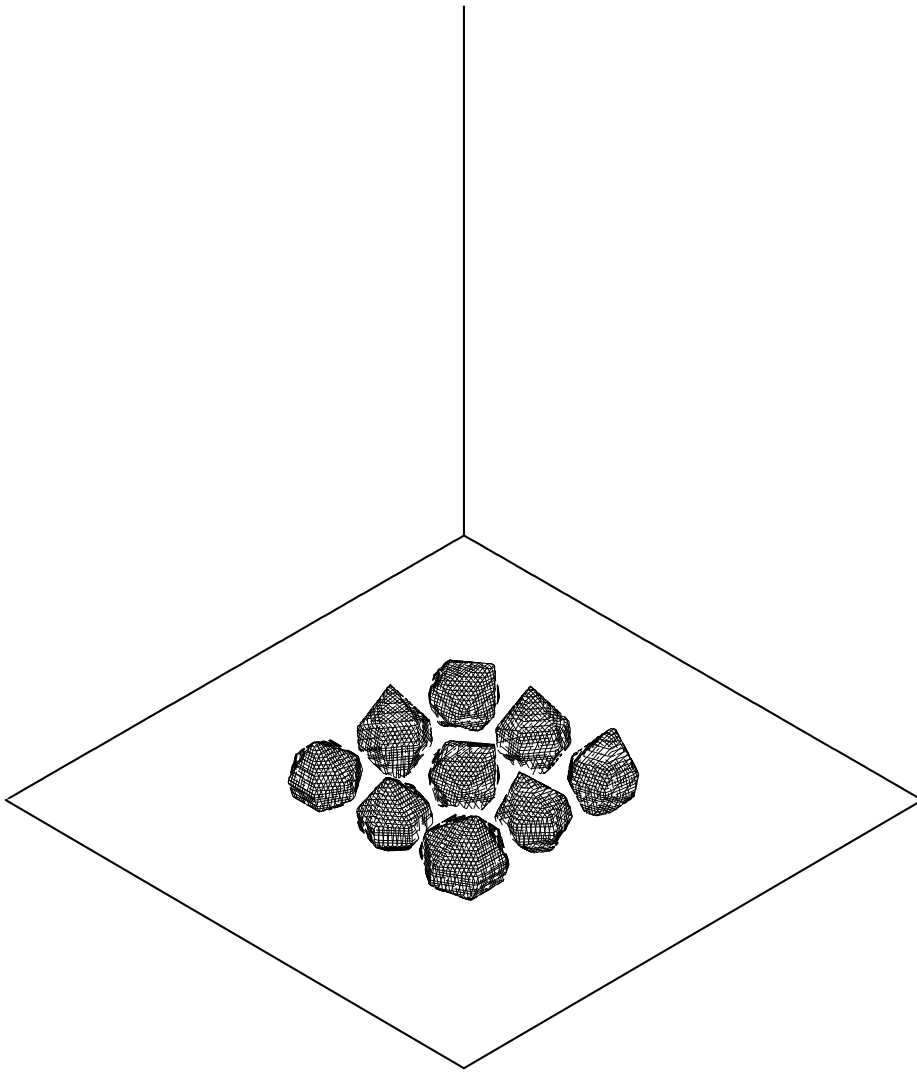


FIG. 20. *Evolution of nine needle-shaped crystals—the initial condition.*

Kolmogorov [12] have studied this problem theoretically and predicted the observed scaling. The vertex tracking algorithm is extremely difficult to implement in three dimensions, whereas our level set approach is very easy to extend to three dimensions.

Three-dimensional tests. Next we consider crystal growth in three dimensions. First we consider the evolution of a single crystal with 14 facets. Six facets (face-facets) are aligned along the faces of a cube and 8 facets (corner-facets) have a normal which is oriented according to the corners of the cube. The facets evolve with two speeds of propagation: v_{100} is the propagation speed for the face-facets and v_{111} is the propagation speed for the 8 corner-facets. The asymptotic shape of a crystal is determined by a single parameter, which is the ratio between the two speeds, $\beta = v_{111}/v_{100}$. If $\beta \leq 1/\sqrt{3}$ then the Wulff shape of the crystal is a regular octahedron; if $\beta \geq \sqrt{3}$, then the Wulff shape is a cube, and for intermediate values of the parameter the asymptotic shape of the crystal is a 14-facet crystal, the relative size of the facets

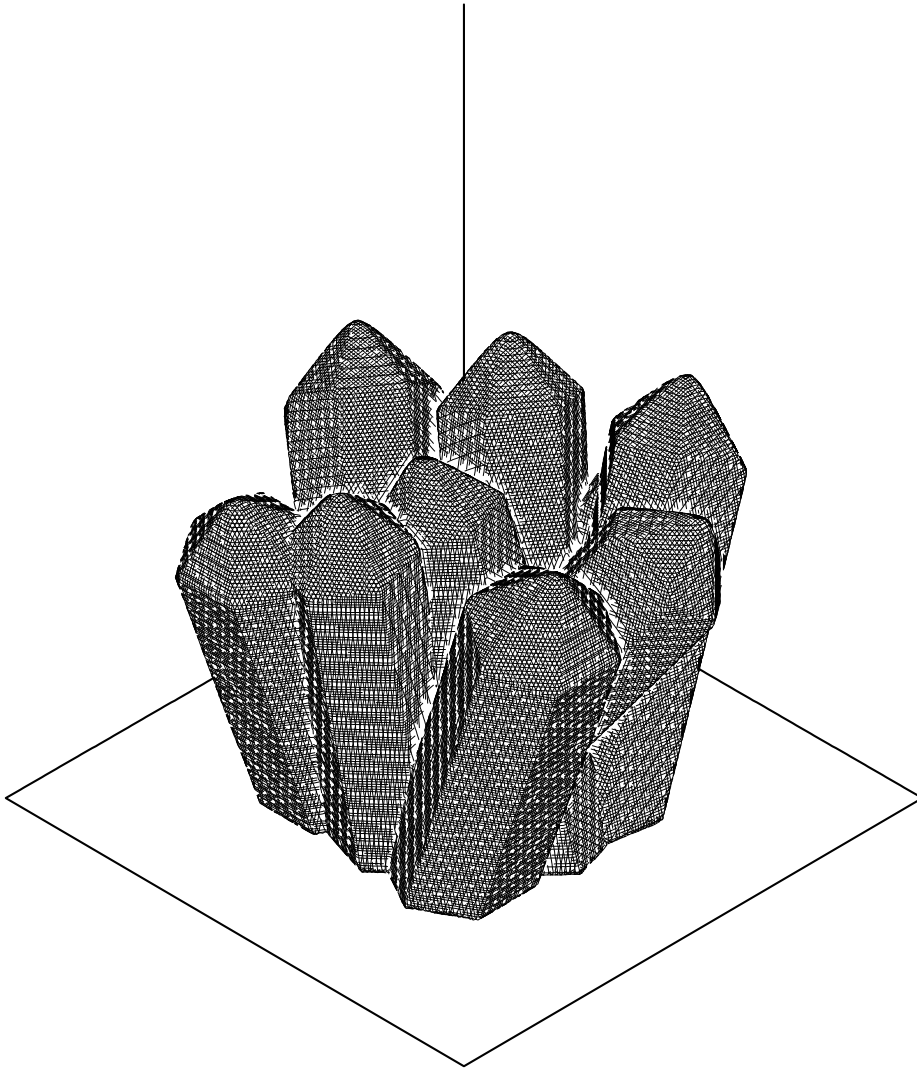


FIG. 21. *Evolution of nine needle-shaped crystals—time $t = 0.72$.*

depending on β . The results of the computation for three different values of β are reported in Figure 15.

Finally, we consider the growth of several crystals in three dimensions. As in the 2D case, when two crystals meet their growth stops and a grain boundary is formed. In the next set of figures (Figures 16–19) we show the evolution of 18 seeds. The crystals are 14-facet crystals with $v_{111}/v_{100} = 1$. The picture shows the zero-level of the phases without making any distinction among them. Here we also see coarsening.

7. Conclusions and future directions. In this paper we have presented a method to evolve faceted interfaces. The scheme is quite simple and robust and can be used for 2D and 3D computations. The method is able to evolve single crystals, as well as polycrystals. The effectiveness of the scheme is shown through several numerical examples. At this stage the method is not very efficient when several

crystals are present, both for cpu time and memory consumption. This is because all the phases are defined in the whole computational domain. More efficient schemes, based on narrow band level set methods, are presently under construction. The new schemes should be one order of magnitude more efficient in the cpu time and two orders of magnitude more efficient in terms of memory usage. We have included a preliminary computation of a polycrystal where the single crystal has a needle-shaped Wulff shape. This crystal has six facets on the long part, and the top and bottom have six facets each. The normal speed of the top and bottom facets is 1, whereas the normal speed of the side facets is 0.2. The initial condition is shown in Figure 20. Here the seeds are like faceted spheres. As the polycrystal evolves the needle shape emerges as shown in Figure 21. This computation was done with a $200 \times 200 \times 200$ mesh using our narrow band method. This would have been almost impossible with our previous method due to time and memory constraints.

Acknowledgments. We thank David Srolovitz and Xingquan Li for helpful conversations. We also thank Stanley Osher for sending us copies of [13, 14].

REFERENCES

- [1] A. VAN DER DRIFT, *Evolutionary selection, a principle governing growth orientation in vapour-deposited layers*, Philips Research Reports, 22 (1967), p. 267.
- [2] D. J. PARITOSH, D. J. SROLOVITZ, C. C. BATTAILE, X. LI, AND J.E. BUTLER, *Simulation of faceted film growth in 2D: Microstructure, morphology and texture*, Acta Materialia, 47 (1999), pp. 2269–2281.
- [3] A. J. DAMMERS AND S. RADELAAR, *2-dimensional computer modeling of polycrystalline film growth*, Texture Microstruct., 14 (1991), pp. 757–762.
- [4] J. E. TAYLOR, *Constructions and conjectures in crystalline nondifferential geometry*, in Differential Geometry, A Symposium in Honor of Manfredo do Carmo, B. Lawson and K. Tenenblat, eds., Longman, Essex, 1991, pp. 321–336.
- [5] J. E. TAYLOR *Motion of curves by crystalline curvature, including triple junctions and boundary points*, Proc. Sympos. Pure Math., 54 (1993), pp. 417–439.
- [6] J. E. TAYLOR, J. CAHN, AND C. A. HANDWERKER, *Geometrical models of crystal growth*, Acta Metallurgica Materialia, 40 (1992), pp. 1443–1474.
- [7] J. CAHN, J. E. TAYLOR, AND C. A. HANDWERKER, *Evolving crystal forms: Frank’s characteristics, revisited*, in Sir Charles Frank OBC, FRS: An Eightieth Birthday Tribute, R. G. Chambers et al., eds., Adam Hilger, Bristol, UK, 1991, pp. 88–118.
- [8] A. HARTEN, *The artificial compression method for computation of shocks and contact discontinuities. I. Single conservation laws*, Comm. Pure Appl. Math., 30 (1977), pp. 611–638.
- [9] G. B. MCFADDEN, A. A. WHEELER, R. BRAUN, S. R. CORIEL, AND R. F. SEKERKA, *Phase-field models for anisotropic interfaces*, Phys. Rev. E, 48 (1993), pp. 2016–2024.
- [10] F. C. FRANK, *On the kinematic theory of crystal growth and dissolution processes. Growth and perfection of crystals*, in Growth and Perfection of Crystals, R.H. Doremus, B.W. Roberts, and D. Turnbull, eds., John Wiley, New York, 1958.
- [11] R. GOGLIONE AND M. PAOLINI, *Numerical Simulation of Crystalline Motion by Mean Curvature with Allen-Cahn Relaxation*, work in progress.
- [12] A. N. KOLMOGOROV, *To the “geometrical selection” of crystals*, Dokl. Acad. Nauk. USSR, 65 (1940), pp. 681–684.
- [13] S. OSHER AND B. MERRIMAN, *The Wulff shape as the asymptotic limit of a growing crystalline interface*, Asian J. Math., 1 (1997), pp. 560–571.
- [14] D. PENG, S. OSHER, B. MERRIMAN, AND H. ZHAO, *The Geometry of Wulff Crystal Shapes and its Relations with Riemann Problems*, UCLA CAM Report 98-51, 1998.
- [15] B. MERRIMAN, J. BENCE, AND S. OSHER, *Motion of multiple junctions: A level set approach*, J. Comput. Phys., 112 (1994), pp. 334–363.
- [16] S. OSHER AND J. SETHIAN, *Fronts propagating with curvature-dependent speed: Algorithms based on Hamilton-Jacobi formulation*, J. Comput. Phys., 79 (1988), pp. 12–49.
- [17] E. ROUY AND A. TOURIN, *A viscosity solutions approach to shape-from-shading*, SIAM J. Numer. Anal., 29 (1992), pp. 867–884.

- [18] J. A. SETHIAN, *A review of the theory, algorithms, and applications of level set methods for propagating interfaces*, in *Acta Numerica*, Cambridge University Press, Cambridge, UK, 1996.
- [19] R. KOBAYASHI, J. A. WARREN, AND W. C. CARTER, *Vector-valued phase field model for crystallization and grain boundary formation*, *Phys. D*, 119 (1998), pp. 415–423.
- [20] L. Q. CHEN AND W. YANG, *Computer simulation of the domain dynamics of a quenched system with large number of nonconserved order parameters: The grain growth kinetics*, *Phys. Rev. B*, 50 (1994), pp. 15752–15756.
- [21] P. SORAVIA, *Generalized motion of a front propagating along its normal direction: A differential games approach*, *Nonlinear Anal.*, 22 (1994), pp. 1247–1262.
- [22] J. E. TAYLOR AND J. W. CAHN, *Diffuse interfaces with sharp corners and facets: Phase field models with strongly anisotropic surfaces*, *Phys. D*, 112 (1998), pp. 381–411.
- [23] J. E. TAYLOR, AND J.W . CAHN, *Linking anisotropic sharp and diffuse surface motion laws via gradient flows*, *J. Statist. Phys.*, 77 (1994), pp. 183–197.
- [24] J. M. THIJSSSEN, H. J. F. KNOPS, AND A. DAMMERS, *Dynamic scaling in polycrystalline growth*, *Phys. Rev. B*, 45 (1992), pp. 8650–8656.
- [25] J. S. WETTLAUFER, M. JACKSON, AND M. ELBAUM, *A geometric model for anisotropic crystal growth*, *J. Phys. A*, 27 (1994), pp. 5957–5967.
- [26] G. WULFF, *Frage der Geschwindigkeit des Wachstums und der Anflösung der Kristallflächen*, *Z. Krystall. Min*, 34 (1901), pp. 449–530.